Research Square

Preprints are preliminary reports that have not undergone peer review.
They should not be considered conclusive, used to inform clinical practice,
or referenced by the media as validated information.

Ambient Environment Adaptive Elastomer Constructed by Microphase Separation and Segment Complexation of Triblock Copolymers

Weijie Wang
Donghua University
Caihong Zhang
Donghua University
Hao Huang
Donghua University
Bing Xue
Donghua University
Shuguang Yang (shgyang@dhu.edu.cn)
Donghua University

Article

Keywords: Adaptive Materials, Elastomer, Hydrogen-bonding Complexation, Microphase Separation, Humidity Sensitivity

Posted Date: July 29th, 2022

DOI: https://doi.org/10.21203/rs.3.rs-1872739/v1

License: This work is licensed under a Creative Commons Attribution 4.0 International License.
Read Full License

Abstract

Elastomers with environmental adaption have attracted considerable attentions for advanced applications in various areas. Here, we fabricate an ambient environment adaptive elastomer by assembling triblock copolymers polystyrene-*b*-poly(acrylic acid)-*b*-polystyrene (SAS) and polystyrene-*b*-poly(ethylene oxide)-*b*-polystyrene (SES). Owing to microphase separation of triblock polymers and hydrogen-bonding complexation of their middle segments, SAS/SES complex presents dichotomy of vitrified hard PS domains and soft PAA/PEO domains which presents major relaxation transition in temperature zone 10–30 ℃ and relative humidity (RH) 40% – 60%. SAS/SES elastomer presents quick adaption to the ambient environment change with temperature and humidity coupling. Moreover, after a loading-unloading cycle training, SAS/SES elastomer exhibits domain orientation, low energy dissipation, high recovery ratio, and distinct strain stiffening compared with the pristine complex. SAS/SES elastomer has potential to be used as sensing and adaption component for complicated intelligent systems.

1. Introduction

Elastomers are soft materials that can withstand large deformation without fracture and spontaneously recover to original dimension after removing the stress.[1, 2] For polymeric elastomer, there are flexible segments that have enough mobility and present as random coil conformation with maximum entropy, and the flexible chain segments are cross-linked, which prevent the permanent flow and make the elastomer obtain the elastic recovery.[3, 4] Cross-linking strategies of elastomers include covalent bond, dynamic covalent bond, and physical associations, such as hydrogen-bonding complex, electrostatic aggregate, hydrophobic domain, and crystalline region.[5–7] These elastomers are essential materials for our daily lives and advanced applications, such as automobile tyre, medical device, footwear, sports goods, space shuttle and satellite.[8, 9]

In living systems, the biological tissues show subtle adaption to surrounding environment and external field.[10, 11] For example, natural skin is initially soft and compliant while shows elastic modulus increasing by several orders of magnitude in a narrow stretching strain change to prevent injury.[12] Inspired by the biological materials, tremendous endeavours have been doing to prepare elastomers with multi-functionality and environment adaption.[13–16] Walther et al. polymerized DNA mechano-probes into elastomers to allow strain-induced fluorescence sensing.[17] Sun et al. constructed robust elastomers with damage resistance and self-healing capacity based on polyurethane (PU) containing poly(dimethylsiloxane) (PDMS), polycaprolactone (PCL) segments and ion liquids doping.[18] Sheiko et al. prepared bottlebrush polymer which shows Young's modulus declining from the GPa to kPa level at a controlled temperature within 28–43 ℃.[19] This materials has potential to be used as tissue adaptive implants that can be inserted as rigid devices followed by matching the surrounding tissue mechanics as a soft elastomer at body temperature.[19]

Triblock copolymers are successful in developing thermoplastic elastomers, such as polystyrene-*b*-polybutadiene-*b*-polystyrene (SBS) and polystyrene-*b*-polyisoprene-*b*-polystyrene (SIS).[20,21] Due to microphase separation, the hard domains of side segments act as the cross-linking junction points while the soft domain of middle segments provides the entropic elasticity. Sheiko et al. reported elastomers of linear-bottlebrush-linear (LBL) triblock copolymer.[22–24] In contrast to the traditional thermoplastic elastomer of linear segment triblock copolymer, the LBL elastomer showed adaptive coloration and tissue-like mechanical properties.[24] Beyond single triblock copolymer, two different triblock copolymers are associated together for complicated hierarchical structure construction and advanced functionality design.[25–28] For example, Hawker et al. synthesized two ABA triblock copolymers, one has positively charged while the other has negatively charged side segments.[25] Based on ionic coacervation of side segments, two ABA triblock copolymers were self-organized in aqueous environment to form hydrogel.[25] Polymer coacervation featured with electrostatic interaction or hydrogen-bonding is sensitive to the environment changes and considered as the basic process analogous to nucleic acid and protein association for genetic information transferring in cell.[29–32] Tirrell et al. systematically studied the properties of oppositely charged ABA triblock copolymers, including coacervation process, rheology behaviours, hierarchical structures, and properties of the resulting hydrogels.[26–28]

Here, we fabricate an ambient environment adaptive elastomer by the strategy of integrating the microphase separation and hydrogen-bonding complexation of two triblock copolymers (Scheme 1). Triblock copolymers, polystyrene-*b*-poly(acrylic acid)-*b*-polystyrene (SAS) and polystyrene-*b*-poly(ethylene oxide)-*b*-polystyrene (SES), are synthesized with controlled free radical polymerization. Poly(acrylic acid) (PAA, middle segment of SAS) and poly(ethylene oxide) (PEO, middle segment of SES) can form hydrogen-bonded complex which is sensitive to environment change.[33–38] Owing to the microphase separation and hydrogen-bonding complexation of middle segments, SAS/SES association presents the dichotomic structures of hard PS domains and soft PAA/PEO hydrogen-bonded polymer complex domains. The hard domains act as the crosslinking junction points and stabilize the whole framework of the material. At room temperature with suitable humidity, SAS/SES complex shows rubber elasticity. By changing temperature and humidity, the strength, stiffness, and toughness of SAS/SES complex can be finely tuned. Pre-drawing make the domain orientation of SAS/SES complex, and subsequently the elastomer shows excellent resilience, low energy dissipation and obvious strain stiffening. SAS/SES elastomer exhibits adaptivity to the ambient environment, and can be used as basic sensing and actuation units for more complicated intelligent systems.

2. Results And Discussion

Triblock copolymers polystyrene-*b*-poly(acrylic acid)-*b*-polystyrene (SAS) and polystyrene-*b*-poly(ethylene oxide)-*b*-polystyrene (SES) were synthesized by reversible addition fragmentation chain transfer polymerization (RAFT) (Supporting Information, **Scheme S1**, **Figure S1-S4**). Four SAS samples are marked as $S_{10k}A_{28k}S_{10k}$, $S_{10k}A_{52k}S_{10k}$, $S_{10k}A_{65k}S_{10k}$, and $S_{10k}A_{120k}S_{10k}$ according to average molecular weight of segments, and their polymer dispersity indexes (PDI) are 1.49, 1.57, 1.60, and 1.61 respectively

(**Table S1**). One SES sample is expressed as $S_{15k}E_{40k}S_{15k,}$ and its PDI is 1.09 (**Table S1**). PS is neither compatible with PAA nor PEO.[39, 40] Here, Four SAS samples and one SES sample all have microphase separation (**Figure S5**).

Table 1
SAS/SES complex samples

Sample	Composition	PS domain content (wt.%)
A1E	$S_{10k}\mathbf{A_{28k}}S_{10k}/S_{15k}E_{40k}S_{15k}$	42.1
A2E	$S_{10k}\mathbf{A_{52k}}S_{10k}/S_{15k}E_{40k}S_{15k}$	34.3
A3E	$S_{10k}\mathbf{A_{65k}}S_{10k}/S_{15k}E_{40k}S_{15k}$	32.2
A4E	$S_{10k}\mathbf{A_{120k}}S_{10k}/S_{15k}E_{40k}S_{15k}$	28.0

SES was associated with four SAS samples separately to prepared the complexes, as listed in Table 1. The length of PEO segments of four SAS/SES complex samples is fixed, and the average polymerization degree is 909. From A1E to A4E, PAA segment becomes long and the polymerization degree are 389, 722, 903, and 1667 in sequence. Due to the incompatibility of PS with PAA and PEO and the hydrogen-bonding complexation of PAA and PEO, SAS/SES complexes present microphase separation structure, one microphase is vitrified PS while the other is PAA/PEO complex (Scheme 1).

Fourier transform infrared spectroscopy (FT-IR) is applied to characterize SAS/SES complexes (Fig. 1a). Spectra of SAS and SES are exhibited as reference. The C = O stretching vibration peak of COOH group in SAS is at 1697 cm^{-1}, while this stretching peak is located at 1725 cm^{-1} in SAS/SES complex. The C-O-C stretching vibration peak of SES before and after association is located at 1102 cm^{-1} and 1083 cm^{-1} respectively. Hydrogen-bonding complexation of PAA segments from SAS and PEO segments from SES make these IR adsorption differences before and after association.[41, 42] Under scrutiny, the wideness and shape of C = O and C-O-C IR adsorption bands of complex samples present variation because PAA segments of SAS triblock copolymers have different length and their complexation with PEO have different hydrogen-bonding degree.

Differential scanning calorimetry (DSC) curves of SAS/SES complexes are displayed in Fig. 1b. They all present two glass transitions, one is from PAA/PEO complexation domain and the other is from PS domain. Glass transition temperature (T_g) of PAA/PEO complexation domain (anhydrous state) is in the temperature region 0–30 ℃. T_g of PS domain is located at temperature zone 95–100 ℃. PAA and PEO have high-level miscibility owing to hydrogen-bonding. PAA/PEO complex only shows one T_g which is located between − 60 ℃ (T_g of PEO) and 106 ℃ (PAA T_g).[33, 43] T_g of PAA/PEO complex is dependent on the composition: the higher PEO content has the lower T_g.[35] T_g of PS domains of SAS/SES complexes have small variation while those of PAA/PEO complexation domains increase as PAA segments become longer. In addition, glass transitions of A3E and A4E are more manifested than those of A1E and A2E. It

indicates that PAA segment length affect composition and size of the PAA/PEO domain and hence the T_g shows the difference.

Small angle X-ray scattering (SAXS) is a classic tool to characterize microphase structure of polymer materials.[44] Basic microphase structures of symmetric triblock polymer (ABA type) are sphere, cylinder, and lamellar.[44–46] The highly ordered microphase structures with long distance correlation need stringent requirements, such as narrow molecular weight distribution and external orientation field.[47, 48] SAXS results (Fig. 1c) reflect the microphase separation of SAS/SES association, while microphase separation structure is not highly ordered due to the molecular weight distribution of SAS samples are relatively broad (PDI > 1.5) and no special external field applied to the pristine SAS/SES complexes.

Stress-strain curves of SAS/SES complexes are shown in Fig. 1d. The mechanical test is conducted at room temperature RH 25%. A1E and A2E exhibit distinct yielding, strain softening, and orientation hardening, like the behaviours of rubber-modified plastics.[49] Compared with A1E and A2E, A3E and A4E have lower PS content. A3E and A4E show the rubber-like tensile behaviours with low modulus and ultimate strain 600% (**Video S1**).

For commercially available thermoplastic elastomer, polystyrene-*b*-polybutadiene-*b*-polystyrene (SBS) or polystyrene-*b*-polyisoprene-*b*-polystyrene (SIS), the PS weight fraction generally is less than 35%.[20, 21] As shown in Table 1, the PS fractions of A3E and A4E are less than 35%, fitting the requirement of hard segment fraction of ABA triblock copolymer thermoplastic elastomer design. In A3E or A4E, PS forms separated hard domain to link the continuous soft domain of PAA/PEO complex. PEO chain is flexible but has strong capability of crystallization. PAA is amorphous polymer and its T_g is higher than 100 ℃.[33, 35] At room temperature, neither PAA nor PEO show rubber-like elastic behaviour. However, the hydrogen-bonded polymer complex of PAA/PEO exhibits as elastomer at room temperature with proper humidity.[33, 36] The crystallization of PEO is restricted by hydrogen-bonding with PAA and the flexibility of PEO retains in the complex matrix. Water molecules adsorbed from the ambient environment act as plasticizer, and hence flexible PAA and PEO have enough mobility. Hydrogen-bonds act as dynamic cross-linking points to prevent permanent flow and obtain recovery force.[2] PAA/PEO complex is stable in acidic environment but will be dissolved in basic solution due to PAA ionization and hydrogen-bond breakage.[50, 51] However, A3E or A4E doesn't dissolve in alkaline solution owing to the cross-linking of PS domain. Though not dissolving in alkaline solution, the hydrogen-bonding between PAA and PEO segments in SAS/SES association is destroyed. After treatment by NaOH solution (0.1 M), the extensibility and toughness of SAS/SES complex greatly reduced (**Figure S6**). Therefore, hydrogen-bonding of PAA and PEO segments is critical not only for microphase separation structure formation process, but also for the mechanical properties of the resulting samples.

IR, DSC and SAXS characterization illustrate micro-phase separation and hydrogen-bonding complexation in SAS/SES assembly systems. Mechanical test demonstrated that A1E and A2E mainly present the behaviours of toughened plastics due to the relatively high PS fraction, while A3E or A4E with

proper PS content has potential to use as elastomer in our daily life ambient environment. Among four SAS/SES complexes, A3E shows the best length matching of PAA and PEO segments in the complexation domain (Table 1), and the subsequently studies are focused on A3E.

Temperature and humidity are two major environmental factors. A3E is characterized by dynamic mechanical analysis (DMA) with temperature scan and humidity scan separately. To demonstrate the pure effect of temperature, the sample was dried in vacuum to completely remove water. The results of DMA temperature scan are shown in Fig. 2a. The storage modulus begins to decrease at 0 ℃, and decreases quickly at 10 ℃. The loss parameter (tan δ) shows a peak around 25 ℃, which is assigned to the glass transition of PAA/PEO complexation domain. The glass transition detected by DMA corresponds to the DSC result in Fig. 1b. The DMA humidity scan is exhibited in Fig. 2b. The storage modulus decreasing initiates at RH 20%, and obviously declining appears at RH 40%. Tan δ begins to increase at RH 20% and shows the peak at RH 55%. It indicates that humidity can induce the mechanical relaxation like temperature. The comfortable living environment for human beings is the temperature between 20 ℃ and 27 ℃, and RH 35% to RH 60%.[52] The major mechanical relaxation of SAS/SES complex soft domain is trigger either by temperature or humidity. If the environment variation with temperature and humidity coupling, the mechanical relaxation will accelerate and become easy.

Tensile stress-strain curves of SAS/SES complex at different RH are shown in Fig. 2c. When treated by vacuum dry, A3E exhibits high initial modulus and breaks at low strain. After incubated in RH 25%, the mechanical behaviours of A3E are quite distinct from the vacuum dried one. A3E exhibits good stretchability and its ultimate strain is about 600%. When RH elevated to 55%, A3E further softens, and its initial modulus and ultimate strength both decrease whereas the ultimate strain increases. Further increasing RH to 90%, A3E becomes extremely soft, and its elongation is high as 1200%.

A3E was incubated in RH 90% at 25 ℃ to obtain water uptake equilibrium, and then was tested under tensile mode at the lower temperature points (10, -10, -20, -30, and − 40 ℃; Fig. 2d). As the temperature decreased, the water in A3E will not lose. A3E shows rubber-like tensile behaviours until cooling down to -20 ℃. At temperature − 30 ℃ or -40 ℃, A3E exhibits the brittle behaviour and breaks at very low strain.

The essence of humidity effect on SAS/SES complex is the interaction of the adsorbed water molecules with the chain segments. The FT-IR spectra of the vacuum dried and the humidified A3E are compared (Fig. 3a). After humidification, the IR peaks of water present, and both the C = O stretching vibration peak of PAA and C-O-C stretching peak of PEO shift, demonstrating the interaction of water with PAA and PEO segments.[53, 54] The equilibrium water content in A3E is determined with TGA (**Figure S7**). The water content as a function of the environmental humidity is shown in Fig. 3b. As humidity increases, there are more water molecules adsorbed into A3E. In the SAS/SES complex, PS domain is hydrophobic while PAA/PEO complex domain is hydrophilic. Therefore, water molecules are mostly involved into PAA/PEO complex domain. Water molecules are plasticizers which can greatly enhance polymer chain mobility. T_g reflects the polymer chain mobility. DSC is a frequently used tool to characterize T_g. However, T_g of the water involved system cannot be determined with general testing protocol which applies the first heating

to high temperature to remove the processing history. Here, the samples are first cooled down to the low temperature to avoid water losing and then heated to detect the glass transition. DSC curves of A3E samples incubated with different humidity environment are shown in Fig. 3c. T_g of the vacuum dried A3E is 25 ℃. As the humidity rises, the more water molecules will be adsorbed and T_g of A3E soft domain will decline. T_g plotted with water content in A3E is shown in Fig. 3d. With 1.0 wt.% water content, T_g drops to 5 ℃. In the complex, water will not be frozen at temperature below 0 ℃ because the water molecules have interactions with PAA and PEO segments and homogeneously distributed. In RH 90%, the equilibrium water content is about 8.5 wt.%, and T_g descends to -25 ℃, which insures that A3E is in rubbery state at room temperature.

The stepwise cyclic loading-unloading tests are performed at RH 25%, RH 55%, and RH 90% separately (Fig. 4a). They all show recovery, energy dissipation, and residue strain. Good resilience under large strain is a typical attribute of elastomer materials. The area between the loading-unloading curves in each cycle is defined as the hysteresis area, which reflects the capability of elastomer to dissipate energy.[55] The ratio between the hysteresis area and the area under the loading curve is referred as damping capacity.[55] The damping capacity for each stretch cycle of A3E at RH 25%, RH 55%, and RH 90% conditions are shown in **Figure S8**. A3E exhibits the higher energy dissipation at RH 25% than at RH 55% and RH 90%. As humidity increasing, more water molecules are adsorbed. Water molecules facilitate the chain mobility in the hydrogen-bonded PAA/PEO domain, which makes the SAS/SES complex have better extensibility. As the maximum strain of the loading-unloading cycle increases, the damping capacity will decrease whereas the declining tendency becomes weak when the strain is above 300% (**Figure S8**). The stress-strain curves of repeating loading-unloading cycles with the fixed maximum strain 300% are shown in Fig. 4b. In first loading-unloading cycle, A3E shows large energy damping. However, in the following cycles, the loop curves almost overlap and the energy dissipation is greatly decreased. SAXS patterns (Fig. 4c**)** show that the pristine A3E has no domain orientation whereas after the first loading-unloading cycle, the orientation presents and retains.

After pre-treatment of drawing to the strain 300%, A3E is retested with loading-unloading cycle mode, as shown in Fig. 4d. The treated A3E has high elastic recovery and low energy dissipation compared with the pristine A3E. The instantaneous elastic recovery is 99%, and damping ratio is about 30% (Fig. 4d) while those of the pristine complex are 81% and 78% respectively. In addition, the treated A3E presents the phenomenon of strain stiffening, which is the characteristic feature of natural elastomer skin that providing a mechanism of self-protection for injury.[23]

In the nature, the pine cone responses to the environment humidity by opening its flaps to release the seeds under favourable growth condition.[11] It is found that SAS/SES complex strip can feel the surrounding temperature and humidity variation and exhibit movement. As illustrated by Fig. 4e and **Video S2**, the A3E strip will reversibly bend and swing to the other side when the finger is close to it. With the same operation, commercially available thermoplastic elastomers SBS or SIS strip do not show swing. Different to SBS and SIS, the soft domain of SAS/SES association is hydrogen-bonded polymer

complex which shows environmental adaptivity. As the finger close to, there is humidity and temperature gradient aside, and hence the different parts present different strength and stiffness, leading to the swing of the strip.

3. Conclusion

In summary, with the association of triblock copolymers of SAS and SES, the ambient environment adaptive elastomer can be fabricated. Owing to micro-phase separation and hydrogen-bonding complexation of the middle segments, SAS/SES complex presents dichotomy of hard domains of PS and soft domains of PAA/PEO complexes. The hard domains act as the junction points of continuous soft domains, which make SAS/SES complex have stability and avoid permanent flow. In contrast to the traditional thermoplastic elastomers, SAS/SES complex shows adaptivity to the ambient environment. Temperature and humidity gradient aside could produce the automatic swing of SAS/SES strip. The extensibility, strength, stiffness, and toughness of SAS/SES elastomer can quickly adapt to the ambient environment variation. After the training of the first loading-unloading cycle, the elastomer presents domain orientation, excellent resilience, low energy dissipation, and strain stiffening. This ambient environment adaptive elastomer has potential to be integrated for more complex autonomous and intelligent material systems.

4. Experimental Section

Materials. Triblock copolymers polystyrene-*b*-poly(acrylic acid)-*b*-polystyrene (SAS) and polystyrene-*b*-poly(ethylene oxide)-*b*-polystyrene (SES) were synthesized by reversible addition fragmentation chain transfer polymerization (RAFT), and the synthesis processes were described in Supporting Information (**Scheme S1**, **Figure S1-S4**, and **Table S1**). *N, N*-dimethylformamide (DMF, 99%, Greagent) dried over $MgSO_4$ with stirring for 24 h and distilled with vacuum line was used as solvent.

SAS/SES Complex. SAS and SES were separately dissolved in anhydrous DMF at concentrations of 10 wt.%. After completely dissolving, two solutions were mixed under strongly stirring for 12 h. The ratio of middle segment repeat units of SAS and SES was controlled at 1:1 ([AA]/[EO] = 1:1). The mixed solution was casted into Teflon mould. The solvent DMF was removed in a vacuum oven at 50 ℃ for over 48 h to obtain the solid SAS/SES complex sample. The SAS/SES complexes prepared with different molecular weight triblock copolymers are listed in Table 1.

Testing and characterization

Tensile testing. The tensile testing of SAS/SES samples was conducted on the universal mechanical testing machine (UTM2103 Shenzhen suns technology Co., Ltd.) at room temperature (25 ℃) with different humidity. The uniaxial tensile speed was 10 mm mim^{-1}. The humidity was controlled by the environment-controlled-chamber. Besides single-loading-test, two cyclic tests were performed. One is repeat the loading-unloading cycle with the maximum strain 300%. The other one is gradually increasing

the tensile strain for loading-unloading cycle. At the first load the strain is 50%, then is with 50% increment after each cycle, and finally the strain increases to 600%.

Dynamic Mechanical Analysis (DMA). The measurement was conducted on TA Q800 machine containing a humidity controlling accessory. For temperature scan, the sample was dried in vacuum before test. The testing temperature increased from − 70 ℃ to 120 ℃ with 10 ℃ min^{-1} heating rate. The humidity scan was conducted from RH 0 to RH 90% at 25 ℃ with humidification rate RH 2% min^{-1}. Either in temperature scan or in humidity scan, the strain and the frequency were set as 0.1% and 1 Hz, respectively. In addition, DMA was used to draw SAS/SES complex sample with equilibrium water uptake in RH 90% at 25 ℃ to conduct tensile test below room temperature (10, -10, -20, -30, and − 40 ℃) with stretching rate 10 mm min^{-1}.

Thermogravimetric Analysis (TGA). TA instrument (Discovery TGA 550) was used to determine the equilibrium water content of SAS/SES complex in different humidity environment. The 4–5 mg SAS/SES complex samples were incubated in humidity controlling chamber for 5 h to obtain water adsorption equilibrium, and then measured with TGA machine immediately. The weight loss before 120 ℃ was used to value water content in SAS/SES.

Differential Scanning Calorimetry (DSC). DSC was performed with TA Discovery DSC 250. Under nitrogen atmosphere with a flowing rate of 50 mL min^{-1}, the heating rate and cooling rate were set as 10 ℃ min^{-1}. The protocol to measure the glass transition temperature (T_g) of SAS/SES without water was: the sample was dried in vacuum before test; increased temperature to 120 ℃ and kept for10 min to eliminate the thermal history, cooled down − 70 ℃ and kept for 3 min, and heated from − 70 ℃ to 120 ℃ to detect thermal events. To avoid water loss, the protocol to measure T_g of water containing SAS/SES complex sample is different. The SAS/SES complexes incubated in different humidity environment was first cooled down to -70 ℃, and then heated up to 120 ℃.

Small Angle X-ray Scattering (SAXS). SAXS patterns were collected at beamline BL16B1 of the Shanghai Synchrotron Radiation Facility. The distance between the sample and detector was 1800 mm. The X-ray wavelength was 0.124 nm and the exposure time was 30 s. The scattering intensity as a function of scattering vector was obtained through radial integration of SAXS pattern with software Fit 2D.

Fourier Transform Infrared Spectroscopy (FT-IR). FT-IR spectra were conducted on a Bruker spectrometer (Vertex 70) with a Single-Bounce ATR attachment. The samples were dried in vacuum oven at 50 ℃ expect for special characterization of humidified sample.

Declarations

Supporting information

The supporting information is available from the author.

Acknowledgement

This work was financially supported by the National Natural Science Foundation of China (No. 51973029), Ministry of Education (No. 8091B022141), and Science and Technology Commission of Shanghai Municipality (No. 20JC1414900).

Conflict of interest

The authors declare no conflict of interest.

References

1. Li, Z.; Zhu, Y. L.; Niu, W.; Yang, X.; Jiang, Z.; Lu, Z. Y.; Liu, X.; Sun, J., Healable and recyclable elastomers with record-high mechanical robustness, unprecedented crack tolerance, and superhigh elastic restorability. Adv. Mater. **33**, 2101498 (2021).
2. Zhuo, Y.; Xia, Z.; Qi, Y.; Sumigawa, T.; Wu, J.; Sestak, P.; Lu, Y.; Hakonsen, V.; Li, T.; Wang, F.; Chen, W.; Xiao, S.; Long, R.; Kitamura, T.; Li, L.; He, J.; Zhang, Z., Simultaneously toughening and stiffening elastomers with octuple hydrogen bonding. Adv. Mater. **33**, 2008523 (2021).
3. Wang, W.; Lu, W.; Goodwin, A.; Wang, H.; Yin, P.; Kang, N. G.; Hong, K.; Mays, J. W., Recent advances in thermoplastic elastomers from living polymerizations: Macromolecular architectures and supramolecular chemistry. Prog. Polym. Sci. **95**, 1–31 (2019).
4. Zhang, H.; Wu, Y.; Yang, J.; Wang, D.; Yu, P.; Lai, C. T.; Shi, A. C.; Wang, J.; Cui, S.; Xiang, J.; Zhao, N.; Xu, J., Superstretchable dynamic polymer networks. Adv. Mater. **31**, 1904029 (2019).
5. Zhou, X.; Guo, B.; Zhang, L.; Hu, G., Progress in bio-inspired sacrificial bonds in artificial polymeric materials. Chem. Soc. Rev. **46**, 6301–6329 (2017).
6. Zhang, Z.; Liu, J.; Li, S.; Gao, K.; Ganesan, V.; Zhang, L., Constructing sacrificial multiple networks to toughen elastomer. Macromolecules **52**, 4154–4168 (2019).
7. Tu, Z.; Liu, W.; Wang, J.; Qiu, X.; Huang, J.; Li, J.; Lou, H., Biomimetic high performance artificial muscle built on sacrificial coordination network and mechanical training process. Nat. Commun. **12**, 2916 (2021).
8. Drobny, J. G., *Handbook of thermoplastic elastomers* - Second Edition, Elsevier, (2014).
9. Krol, P., Synthesis methods, chemical structures and phase structures of linear polyurethanes. Properties and applications of linear polyurethanes in polyurethane elastomers, copolymers and ionomers. Prog. Mater. Sci. **52**, 915–1015 (2007).
10. Merindol, R.; Walther, A., Materials learning from life: concepts for active, adaptive and autonomous molecular systems. Chem. Soc. Rev. **46**, 5588–5619 (2017).

11. Walther, A., Viewpoint: From responsive to adaptive and interactive materials and materials systems: A roadmap. Adv. Mater. **32**, 1905111 (2020).
12. Meyers, M. A.; Chen, P. Y.; Lin, A. Y. M.; Seki, Y., Biological materials: Structure and mechanical properties. Prog. Mater. Sci. **53**, 1–206 (2008).
13. Zhang, Y.; Ye, S.; Cao, L.; Lv, Z.; Ren, J.; Shao, Z.; Yao, Y.; Ling, S., Natural silk spinning-inspired meso-assembly-processing engineering strategy for fabricating soft tissue-mimicking biomaterials. Adv. Funct. Mater. **32**, 2200267 (2022).
14. Yu, Y.; Kong, K.; Tang, R.; Liu, Z., A bioinspired ultratough composite produced by integration of inorganic ionic oligomers within polymer networks. ACS Nano **16**, 7926–7936 (2022).
15. Zhang, Z.; Cheng, L.; Zhao, J.; Zhang, H.; Zhao, X.; Liu, Y.; Bai, R.; Pan, H.; Yu, W.; Yan, X., Muscle-mimetic synergistic covalent and supramolecular polymers: Phototriggered formation leads to mechanical performance boost. J. Am. Chem. Soc. **143**, 902–911 (2021).
16. He, W.; Qian, D.; Wang, Y.; Zhang, G.; Cheng, Y.; Hu, X.; Wen, K.; Wang, M.; Liu, Z.; Zhou, X.; Zhu, M., A protein-like nanogel for spinning hierarchically structured artificial spider silk. Adv. Mater. 2201843 (2022).
17. Creusen, G.; Schmidt, R. S.; Walther, A., One-component DNA mechanoprobes for facile mechanosensing in photopolymerized hydrogels and elastomers. ACS Macro Lett. **10**, 671–678 (2021).
18. Wang, X.; Zhan, S.; Lu, Z.; Li, J.; Yang, X.; Qiao, Y.; Men, Y.; Sun, J., Healable, recyclable, and mechanically tough polyurethane elastomers with exceptional damage tolerance. Adv. Mater. **32**, 2005759 (2020).
19. Zhang, D.; Dashtimoghadam, E.; Fahimipour, F.; Hu, X.; Li, Q.; Bersenev, E. A.; Ivanov, D. A.; Varnoosfaderani, M. V.; Sheiko, S. S., Tissue-adaptive materials with independently regulated modulus and transition temperature. Adv. Mater. **32**, 2005314 (2020).
20. Holden, G., Thermoplastic Elastomers. Applied Plastics Engineering Handbook, 2017, pp 91–107.
21. Puskas, J. E.; Kaszas, G., Polyisobutylene-based thermoplastic elastomers: A review. Rubber Chem. Technol. **69**, 462–475 (1996).
22. Varnosfaderani, M. V.; Daniel, W. F. M.; Everhart, M. H.; Pandya, A. A.; Liang, H.; Matyjaszewski, K.; Dobrynin, A. V.; Sheiko, S. S., Mimicking biological stress-strain behaviour with synthetic elastomers. Nature **549**, 497–501 (2017).
23. Sheiko, S. S.; Dobrynin, A. V., Architectural code for rubber elasticity: From supersoft to superfirm materials. Macromolecules **52**, 7531–7546 (2019).
24. Varnosfaderani, M. V.; Keith, A. N.; Cong, Y.; Liang, H.; Rosenthal, M.; Sztucki, M.; Clair, C.; Magonov, S.; Ivanov, D. A.; Dobrynin, A. V.; Sheiko, S. S., Chameleon-like elastomers with molecularly encoded strain-adaptive stiffening and coloration. Science **359**, 1509–1513 (2018).
25. Hunt, J. N.; Feldman, K. E.; Lynd, N. A.; Deek, J.; Campos, L. M.; Spruell, J. M.; Hernandez, B. M.; Kramer, E. J.; Hawker, C. J., Tunable, high modulus hydrogels driven by ionic coacervation. Adv. Mater. **23**, 2327–2331 (2011).

26. Srivastava, S.; Levi, A. E.; Goldfeld, D. J.; Tirrell, M. V., Structure, morphology, and rheology of polyelectrolyte complex hydrogels formed by self-assembly of oppositely charged triblock polyelectrolytes. Macromolecules **53**, 5763–5774 (2020).
27. Srivastava, S.; Andreev, M.; Levi, A. E.; Goldfeld, D. J.; Mao, J.; Heller, W. T.; Prabhu, V. M.; de Pablo, J. J.; Tirrell, M. V., Gel phase formation in dilute triblock copolyelectrolyte complexes. Nat. Commun. **8**, 14131 (2017).
28. Li, D. F.; Gockler, T.; Schepers, U.; Srivastava, S., Polyelectrolyte complex-covalent interpenetrating polymer network hydrogels. Macromolecules **55**, 4481–4491 (2022).
29. Sing, C. E.; Perry, S. L., Recent progress in the science of complex coacervation. Soft Matter **16**, 2885–2914 (2020).
30. Schaaf, P.; Schlenoff, J. B., Saloplastics: Processing compact polyelectrolyte complexes. Adv. Mater. **27**, 2420–2432 (2015).
31. Klosin, A.; Hyman, A. A., A liquid reservoir for silent chromatin. Nature *547*, 168–169 (2017).
32. Lutz, J. F.; Lehn, J. M.; Meijer, E. W.; Matyjaszewski, K., From precision polymers to complex materials and systems. Nat. Rev. Mater. **1**, 16024 (2016).
33. Wang, Y.; Liu, X.; Li, S.; Li, T.; Song, Y.; Li, Z.; Zhang, W.; Sun, J., Transparent, healable elastomers with high mechanical strength and elasticity derived from hydrogen-bonded polymer complexes. ACS Appl. Mater. Interfaces **9**, 29120–29129 (2017).
34. Qin, S.; Song, Y.; Floto, M. E.; Grunlan, J. C., Combined high stretchability and gas barrier in hydrogen-bonded multilayer nanobrick wall thin films. ACS Appl. Mater. Interfaces **9**, 7903–7907 (2017).
35. Li, J.; Wang, Z.; Wen, L.; Nie, J.; Yang, S.; Xu, J.; Cheng, S. Z. D., Highly elastic fibers made from hydrogen-bonded polymer complex. ACS Macro Lett. **5**, 814–818 (2016).
36. Lutkenhaus, J. L.; Hrabak, K. D.; McEnnis, K.; Hammond, P. T., Elastomeric flexible free-standing hydrogen-bonded nanoscale assemblies. J. Am. Chem. Soc. **127**, 17228–17234 (2005).
37. Miyoshi, T.; Takegoshi, K.; Hikichi, K., High-resolution solid state 13C n.m.r. study of the interpolymer interaction, morphology and chain dynamics of the poly(acrylic acid)/poly(ethylene oxide) complex. Polymer **38**, 2315–2320 (1997).
38. Wang, W.; Xu, X.; Zhang, C.; Huang, H.; Zhu, L.; Yue, K.; Zhu, M.; Yang, S., Skeletal muscle fibers inspired polymeric actuator by assembly of triblock polymers. Adv. Sci. **9**, 2105764 (2022).
39. Xu, H. Y.; Greve, E. M.; Mahanthappa, M. K., Morphological impact of segment dispersity in lithium salt-doped poly(styrene)/poly(ethylene oxide) triblock polymers. Macromolecules **52**, 5722–5734 (2019).
40. Ribeiro, T.; Prazeres, T. J. V.; Moffitt, M.; Farinha, J. P. S., Enhanced photoluminescence from micellar assemblies of cadmium sulfide quantum dots and gold nanoparticles. J. Phys. Chem. C **117**, 3122–3133 (2013).
41. Li, J.; Sun, J.; Wu, D.; Huang, W.; Zhu, M.; Reichmanis, E.; Yang, S., Functionalization-directed stabilization of hydrogen-bonded polymer complex fibers: Elasticity and conductivity. Adv. Fiber

Mater. **1**, 71–81 (2019).

42. Sukhishvili, S. A.; Granick, S., Layered, erasable polymer multilayers formed by hydrogen-bonded sequential self-assembly. Macromolecules **35**, 301–310 (2002).
43. Zhu, M.; Wang, W.; Zhang, C.; Zhu, L.; Yang, S., Photo-responsive behaviors of hydrogen-bonded polymer complex fibers containing azobenzene functional groups. Adv. Fiber Mater. **3**, 172–179 (2021).
44. Su, Z.; Zhang, R.; Yan, X. Y.; Guo, Q. Y.; Huang, J.; Shan, W.; Liu, Y.; Liu, T.; Huang, M.; Cheng, S. Z. D., The role of architectural engineering in macromolecular self-assemblies via non-covalent interactions: A molecular LEGO approach. Prog. Polym. Sci. **103**, 101230 (2020).
45. Abetz, V.; Simon, P. F. W., Phase behaviour and morphologies of block copolymers. Adv. Polym. Sci. **189**, 125–212 (2005).
46. Matsen, M. W.; Thompson, R. B., Equilibrium behavior of symmetric ABA triblock copolymer melts. J. Chem. Phys. **111**, 7139–7146 (1999).
47. Honeker, C. C.; Thomas, E. L., Impact of morphological orientation in determining mechanical properties in triblock copolymer systems. Chem. Mater. **8**, 1702–1714 (1996).
48. Lynd, N. A.; Meuler, A. J.; Hillmyer, M. A., Polydispersity and block copolymer self-assembly. Prog. Polym. Sci. **33**, 875–893 (2008).
49. Caldona, E. B.; De Leon, A. C. C.; Pajarito, B. B.; Advincula, R. C., A review on rubber-enhanced polymeric materials. Polym. Rev. **57**, 311–338 (2016).
50. Kharlampieva, E.; Kozlovskaya, V.; Sukhishvili, S. A., Layer-by-layer hydrogen-bonded polymer films: From fundamentals to applications. Adv. Mater. **21**, 3053–3065 (2009).
51. Ma, S.; Qi, X.; Cao, Y.; Yang, S.; Xu, J., Hydrogen bond detachment in polymer complexes. Polymer **54**, 5382–5390 (2013).
52. Zhang, X.; Chao, X.; Lou, L.; Fan, J.; Chen, Q.; Li, B.; Ye, L.; Shou, D., Personal thermal management by thermally conductive composites: A review. Compos. Commun. **23**, 100595 (2021).
53. Hou, Y.; Guan, Q. F.; Xia, J.; Ling, Z. C.; He, Z.; Han, Z. M.; Yang, H. B.; Gu, P.; Zhu, Y.; Yu, S. H.; Wu, H., Strengthening and toughening hierarchical nanocellulose via humidity-mediated interface. ACS Nano **15**, 1310–1320 (2021).
54. Liu, Y.; Xu, B.; Sun, S.; Wei, J.; Wu, L.; Yu, Y., Humidity- and photo-induced mechanical actuation of cross-linked liquid crystal polymers. Adv. Mater. **29**, 1604792 (2017).
55. Zhu, Y.; Shen, Q.; Wei, L.; Fu, X.; Huang, C.; Zhu, Y.; Zhao, L.; Huang, G.; Wu, J., Ultra-tough, strong, and defect-tolerant elastomers with self-healing and intelligent-responsive abilities. ACS Appl. Mater. Interfaces **11**, 29373–29381 (2019). **TOC**:

Schemes

Scheme 1 is available in the supplementary files section.

Figures

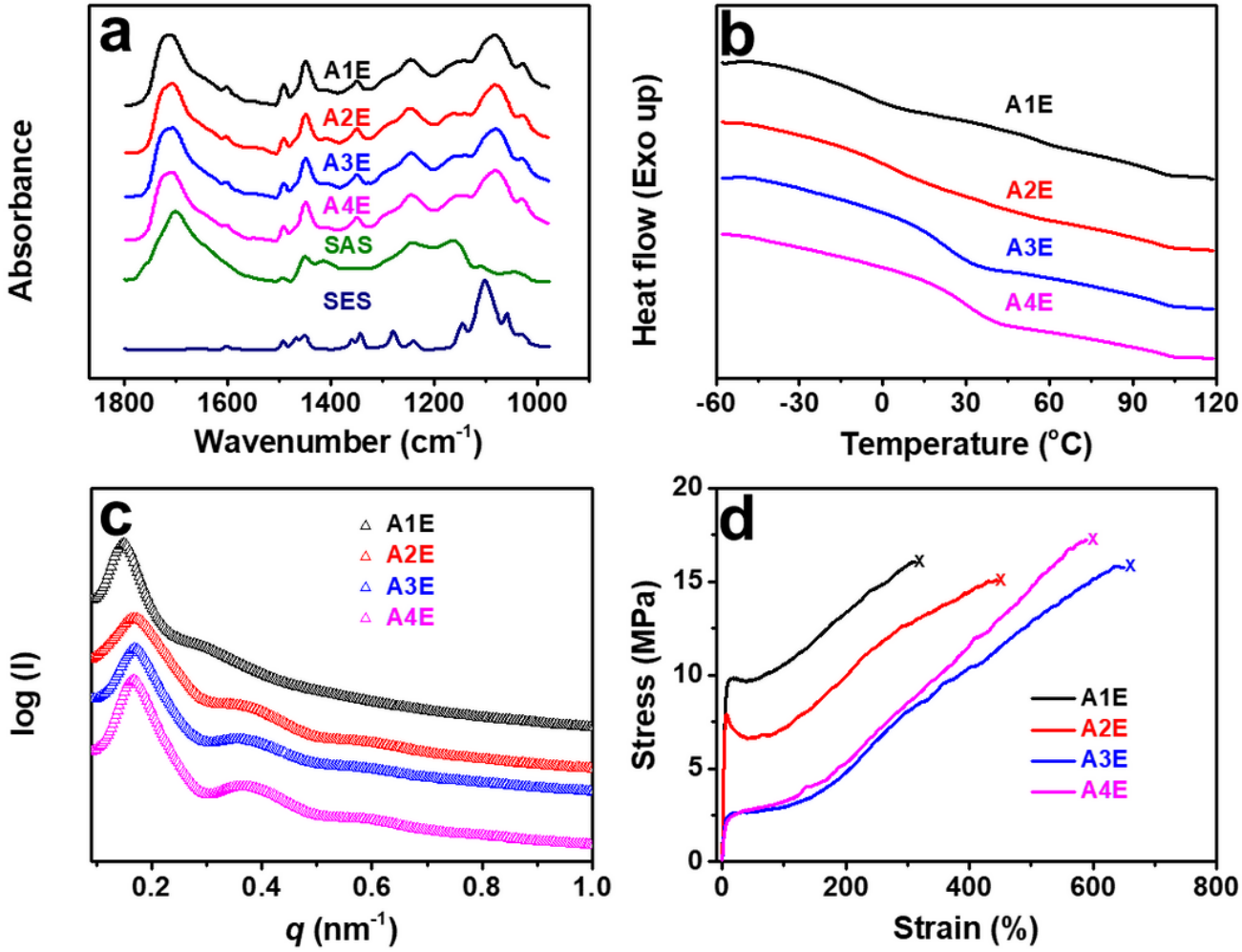

Figure 1

a) FT-IR spectra, **b)** DSC curves, **c)** SAXS curves, and **d)** stress-strain curves of pristine A1E, A2E, A3E, and A4E. The triblock copolymers of SAS and SES are compared in FT-IR spectra. The tensile testing was conducted at 25 °C and relative humidity (RH) 25%.

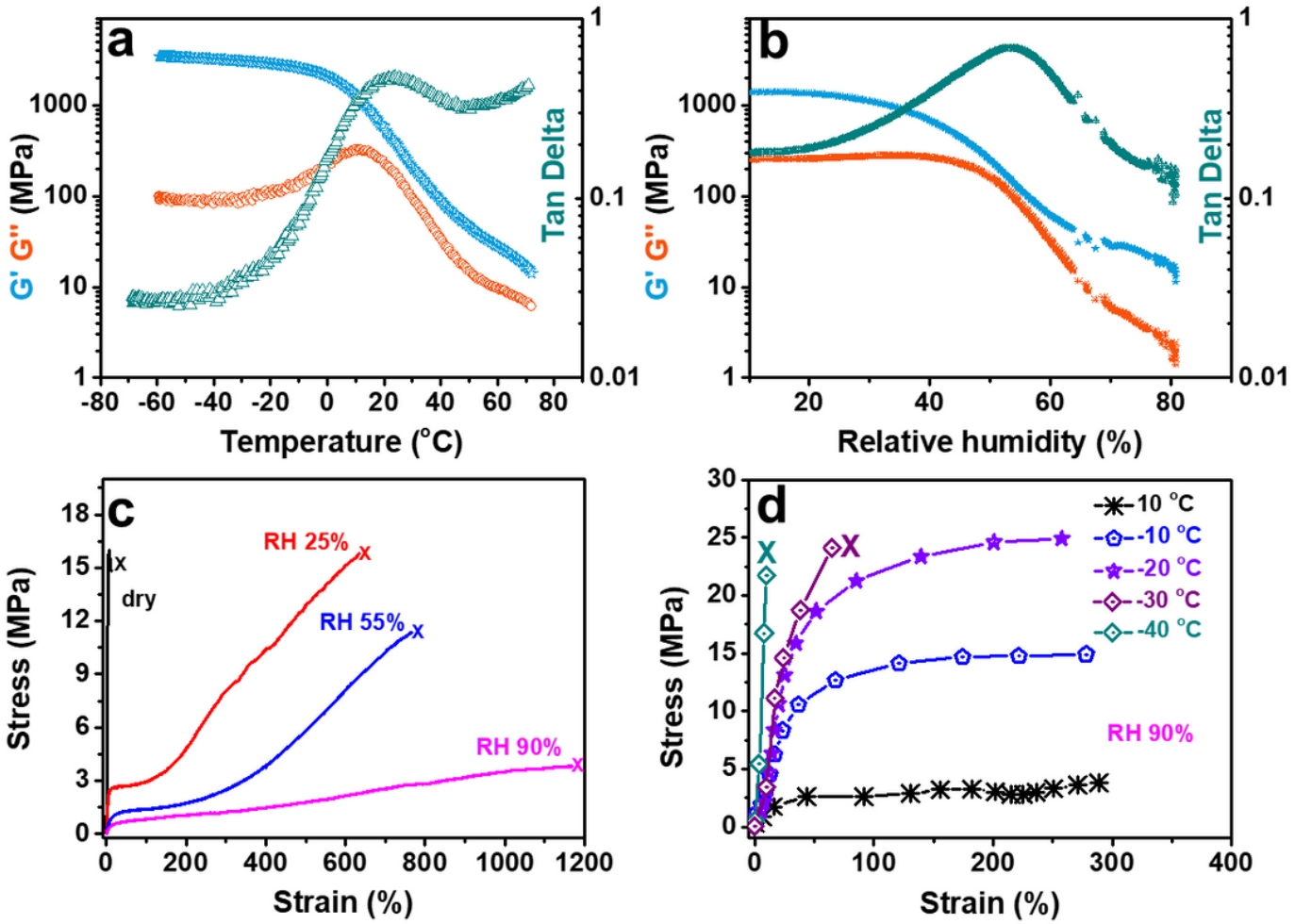

Figure 2

a) DMA curves of A3E, the temperature scan. **b)** DMA curves of A3E, humidity scan at 25 ℃. **c)** Stress-strain curves of A3E at different relative humidity (RH) conditions with tensile machine. **d)** Stress-strain curves of A3E which were incubated in the environment of 25 ℃ and RH 90% to obtain water uptake equilibrium then tested with DMA under stretching mode (maximum testing strain 300%) at the lower temperature points.

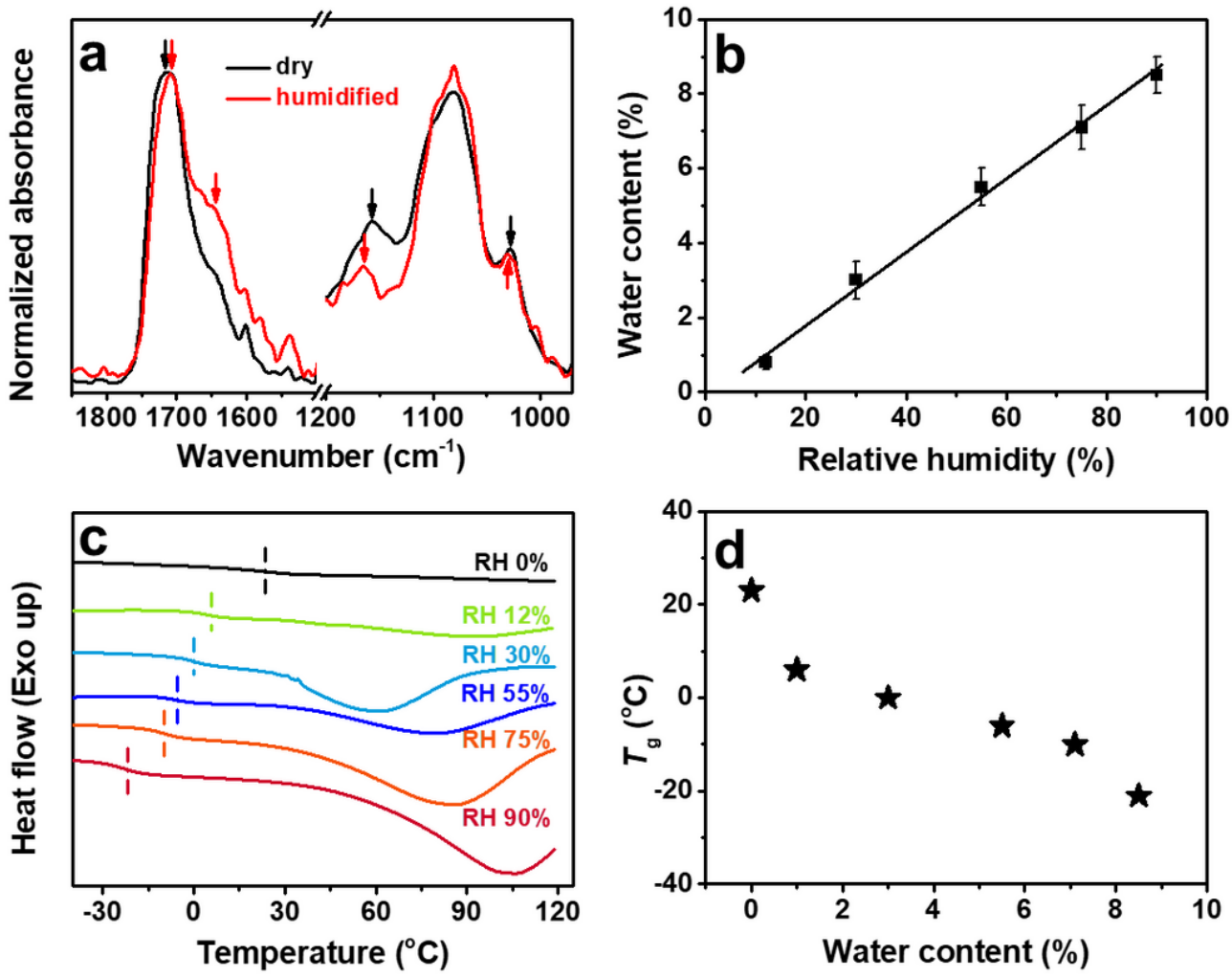

Figure 3

a) FT-IR spectra of dry A3E and humidified A3E illustrate the effect of water molecules on the hydrogen-bond. **b)** Water content of A3E at different RH conditions. **c)** DSC curves of A3E at different RH conditions. **d)** Changes in T_g as the function of water content in A3E.

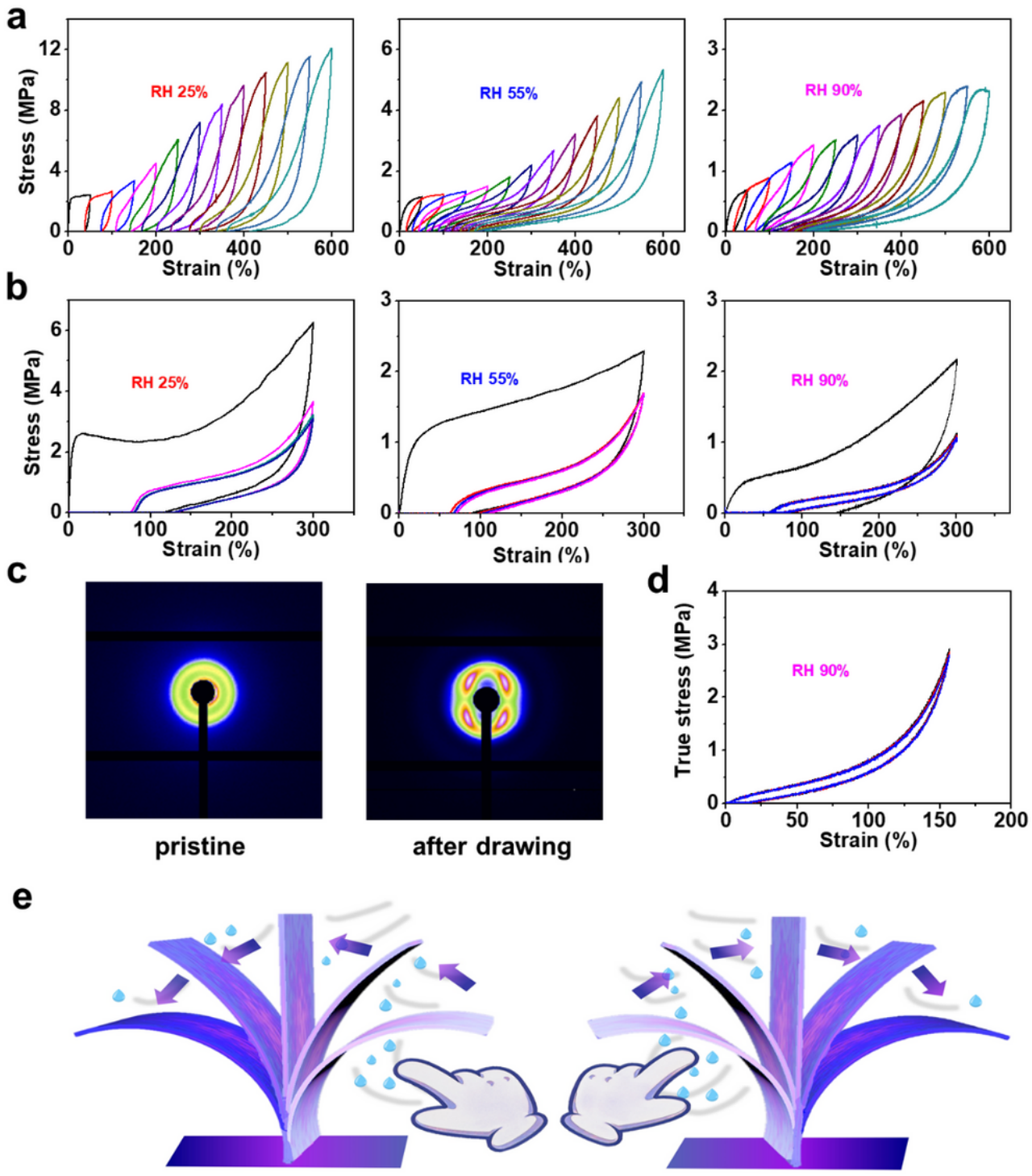

Figure 4

a) Step cyclic loading-unloading curves of A3E at 25 °C but different RH conditions. Each cycle strain increases by 50% and until reaches to 600%. **b)** Repeating loading-unloading curves of A3E with maximum strain 300% at 25 °C but different RH conditions. A3E was stretched to 300% strain and returned to the initial length, then conducted to the next cycle and training for several times to improve its elasticity. The black curve is the first cycle. **c)** 2D SAXS patterns of pristine and after drawing A3E

(elongation strain 300%). **d)** True stress-strain cyclic loading-unloading curves of A3E after training. **e)** Scheme shows A3E strip will reversibly bend and swing when the finger closes.

Supplementary Files

This is a list of supplementary files associated with this preprint. Click to download.

- SupportingInformation20220719.docx
- VideoS1.mp4
- VideoS2.mp4
- floatimage1.png
- floatimage6.jpeg